

# A transient component in the pulse profile of PSR J0738–4042

A. Karastergiou<sup>1</sup>, S. J. Roberts<sup>2</sup>, S. Johnston<sup>3</sup>, H. Lee<sup>2</sup>, P. Weltevrede<sup>4</sup> and M. Kramer<sup>5</sup>

<sup>1</sup>*Astrophysics, University of Oxford, Denys Wilkinson Building, Keble Road, Oxford OX1 3RH, UK*

<sup>2</sup>*Information Engineering, University of Oxford, Parks Road, Oxford OX1 3PJ, UK*

<sup>3</sup>*Australia Telescope National Facility, CSIRO, P.O. Box 76, Epping, NSW 1710, Australia*

<sup>4</sup>*Jodrell Bank Centre for Astrophysics, The University of Manchester, Alan Turing Building, Manchester, M13 9PL, United Kingdom*

<sup>5</sup>*Max-Planck-Institut für Radioastronomie, Auf dem Huegel 69, 53121 Bonn, Germany*

14 March 2011

## ABSTRACT

One of the tenets of the radio pulsar observational picture is that the integrated pulse profiles are constant with time. This assumption underpins much of the fantastic science made possible via pulsar timing. Over the past few years, however, this assumption has come under question with a number of pulsars showing pulse shape changes on a range of timescales. Here, we show the dramatic appearance of a bright component in the pulse profile of PSR J0738–4042 (B0736–40). The component arises on the leading edge of the profile. It was not present in 2004 but strongly present in 2006 and all observations thereafter. A subsequent search through the literature shows the additional component varies in flux density over timescales of decades. We show that the polarization properties of the transient component are consistent with the picture of competing orthogonal polarization modes. Faced with the general problem of identifying and characterising average profile changes, we outline and apply a statistical technique based on a Hidden Markov Model. The value of this technique is established through simulations, and is shown to work successfully in the case of low signal-to-noise profiles.

**Key words:** pulsars: individual: J0738–4042, B0736–40

## 1 INTRODUCTION

The radio emission from pulsars is characterised by a range of dynamic phenomena that take place on various timescales. Microstructure is observed at the shortest ( $\mu\text{s}$ ) timescales, stochastic or organised changes in the pulse shape occur on timescales of the rotational period  $P$ , while other phenomena such as nulling (e.g. Lorimer & Kramer 2005), where radio emission totally switches off, may last significantly longer than one rotation. An examination of the average pulse properties of a given pulsar however, demonstrates that the mean shape of a sufficiently large number of individual pulses remains remarkably constant over long periods of time. It is this quality of radio pulsars that makes them extremely useful tools: knowing the exact shape of the pulse profile increases the precision of the measurement of the pulse time of arrival, which is the basic quantity in pulsar timing experiments.

Although it is rare that the integrated profiles of pulsars change with time, it is not unprecedented. Timescales of changes range from hours through to months and years. On short timescales are the rotating radio transients (RRATs)

(McLaughlin et al. 2006), which are thought to be neutron stars that only emit individual bursts of emission at irregular and infrequent intervals. A group of pulsars show mode changing, where two distinct and different pulse profiles are observed over timescales of hours (e.g. Gil et al. 1994). The intermittent pulsar PSR B1931+24 (Kramer et al. 2006) is present for 5 to 10 days before its emission ceases for some 30 days. In this case, the derivative of the rotational period,  $\dot{P}$ , changes between the on and off phases and is therefore correlated with changes in the radio pulse profile. Similar results associated with more subtle profile changes are reported in Lyne et al. (2010), and another intermittent pulsar (PSR J1832+0029) is discussed in Kramer et al. (2008). In PSR J1119–6127 pulse changes were seen which appeared to be associated with glitch activity (Weltevrede et al. 2011). There is strong evidence that all these effects (nulling, mode changing and intermittency) are magnetospheric in origin.

A further long-term effect, due to geodetic precession of a pulsar in a binary orbit, can also cause pulse shape changes. These have been observed in e.g. PSR B1913+16 (Kramer 1998, Weisberg & Taylor 2002) and J1141–6545

arXiv:1103.2247v1 [astro-ph.HE] 11 Mar 2011

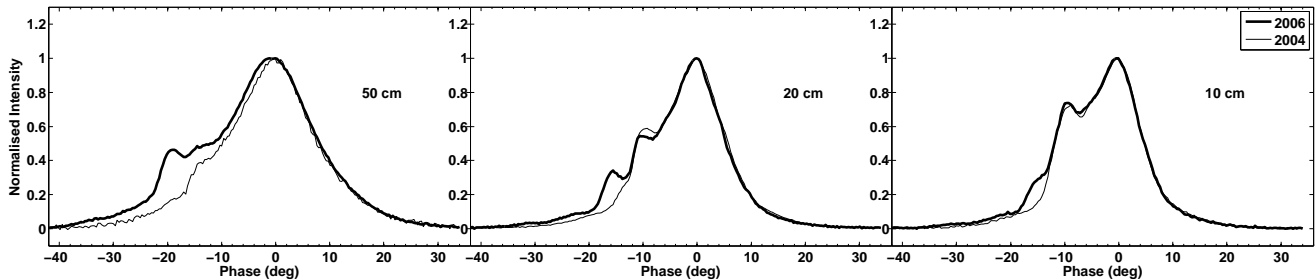


**Figure 1.** The average profile of PSR J0738–4042 as observed with the 50, 20 and 10 cm receivers at Parkes, in the first half of 2004 (thin line) and the second half of 2006 (thick line). The change in the leading edge of the profile shape is visible at all frequencies.

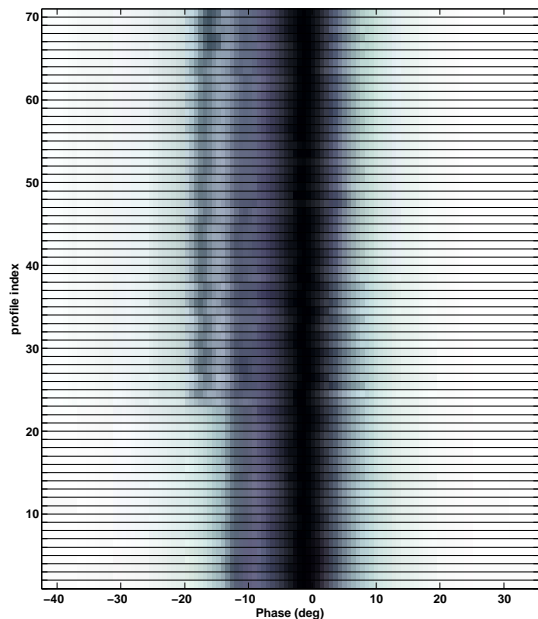


**Figure 2.** A greyscale representation of the intensity of 71 profiles, observed at *irregular* intervals between 2003 and 2011. The peak intensity of each profile is normalised to unity; the profiles are aligned by cross-correlation with a top-hat function. The change occurs at profile 23.

(Manchester et al. 2010). Periodic changes in the average profile of PSR B1828–11 were interpreted as free precession by Stairs et al. (2000), however free precession of solitary neutron stars is considered unlikely (Sedrakian et al. 1999) on theoretical grounds. Changes in the pulse profile due to precession relate to changes in the viewing geometry rather than magnetospheric effects.

The average pulse profiles of pulsars are partially linearly polarized, to a lesser or higher degree. Highly energetic pulsars feature high degrees of linear polarization (e.g. Weltevrede & Johnston 2008). There is good evidence to suggest that the observed emission results from the superposition of two orthogonally polarized modes (OPM), which arise and propagate inside the pulsar magnetosphere (e.g. McKinnon & Stinebring 2000, Karastergiou et al. 2001). Comparable intensities of the modes has been favoured observationally

as the cause for reduced linear polarization in pulsars at typical ( $\sim 1$  GHz) observing frequencies. A further observational consequence is that the changes in the structure of the total power average profile with observing frequency are often coupled with particular changes in the degree of linear polarization, reflecting the spectral behaviour of the orthogonal polarization modes (as discussed in Karastergiou et al. 2005, Smits et al. 2006); as the OPMs become more equal in strength, the total power increases and the polarization decreases.

Pulsar timing models need to incorporate all known physical phenomena (intrinsic to the pulsar or not) that affect the measured times-of-arrival, in order to achieve a floor of sensitivity that would enable the discovery of extremely weak components to the model, such as gravitational waves (e.g. Hobbs et al. 2009). Pulsar timing uses template matching and relies on the average profile not varying with time. Any variability in the profile adversely affect the timing model. In the following, we present data from a significant change in the average pulse profile of PSR J0738–4042. We show how polarization data reveal details about the change, and discuss possible interpretations. We present a robust statistical technique to characterise the change, and explore its potential physical origins.

## 2 THE TOTAL INTENSITY PROFILE OF PSR J0738–4042

PSR J0738–4042 was one of the first radio pulsars discovered (Large et al. 1968). It has a high dispersion measure of  $160.8 \text{ cm}^{-3} \text{ pc}$ , and its spin period of  $P = 375 \text{ ms}$  and a period derivative of  $\dot{P} = 1.61 \times 10^{-15}$  places it within the bulk of normal pulsars on the  $P$ - $\dot{P}$  diagram. Its relatively high flux density (80 mJy at 1.4 GHz) has made it a consistent observing target over the 40 years since its discovery. The most recent polarimetric profiles of the pulsar over a wide range of frequencies have been published in Karastergiou & Johnston (2006), Johnston et al. (2006) and Johnston et al. (2007). Average profiles in three separate observing bands taken in 2004 are shown in Fig. 1 (thin line). The profile at 1.4 GHz shows one bright component with a shoulder component on its leading edge, on what appears to be a broad pedestal of emission on the leading and trailing edge. Subsequently, the pulsar was observed as part of a program to measure accurate rotation measures (Noutsos et al. 2009). The 1.4 GHz profile, taken in 2006, is shown as the thick line in Fig. 1. An additional component,  $\approx 15^\circ$  earlier than the

**Table 1.** 40 years of average profiles from PSR J0738–4042.

Date	Frequency	Component at $-15^\circ$	Reference
<1970	1720 MHz	Strong and discrete	Komesaroff et al (1970)
<1975	1400 MHz	Strong and discrete	Backer (1976)
<1977	631 MHz	Shoulder to main pulse	McCulloch et al.(1978)
<1977	1612 MHz	Strong and discrete	Manchester et al. (1980)
1979	950 MHz	Strong and discrete	van Ommen et al. (1997)
1990	950 MHz	Weak shoulder to main pulse	van Ommen et al. (1997)
1991	800 MHz	Absent	van Ommen et al. (1997)
1996	1375 MHz	Absent	unpublished
1997	1375 MHz	Absent	unpublished
2004	1375 MHz	Absent	Karastergiou & Johnston (2006)
2004	3100 MHz	Absent	Karastergiou & Johnston (2006)
2005	8400 MHz	Absent	Johnston et al. (2006)
2005	3100 MHz	Absent	Johnston et al. (2007)
2006	1369 MHz	Strong and discrete	Noutsos et al. (2009)

main peak, can be seen on the leading edge of the 2006 profile, which is almost entirely absent in 2004. This component is present at all three observing frequencies.

Armed with this result, we looked through the literature for other published profiles of this pulsar. Table 1 includes a summary of available data, where the date and observing frequency are given with a note relating to the presence of the leading component. Two facts are immediately evident. First, there is a period between 1991 and 2005 where the component is totally absent. Secondly, the presence or absence of the leading component is a broadband phenomenon; there are no contradictory observations at a particular frequency. This is clearly seen in the representative, high S/N profiles in Fig. 1, all showing additional leading edge emission in 2006.

Figure 2 shows data from 71 pulse profiles taken with the 21 cm receiver of the Parkes telescope. The profiles, which are not collected at regular intervals, span a range of dates from February 2003 to January 2011. The index of each profile as shown on the y-axis is used for the statistical analysis that follows. The duration of each observation varies from 120 to 1199 s. All profiles in Fig. 2 have been normalised to the peak intensity and aligned by cross correlation with a top hat function. Although absolute flux density calibration is not available for all observations, an analysis of the S/N as a function of observing time reveals that the peak flux density remains broadly similar, within a  $\approx 20\%$  margin. The crucial change in the shape of the leading edge can be clearly detected after profile #23 with the “new” component remaining on all subsequent profiles. Towards the end of the sequence the new component has grown to its brightest amplitude.

### 3 CHANGES IN THE POLARIZATION PROFILE

As mentioned in the introduction, polarization is a useful diagnostic in the interpretation of pulsar radio emissions. Figure 3 shows three average profiles of PSR J0738–4042, from 2004, 2006 and 2010. It is immediately obvious that the additional component which appears between 2004 and 2006 is also associated with a different polarization state.

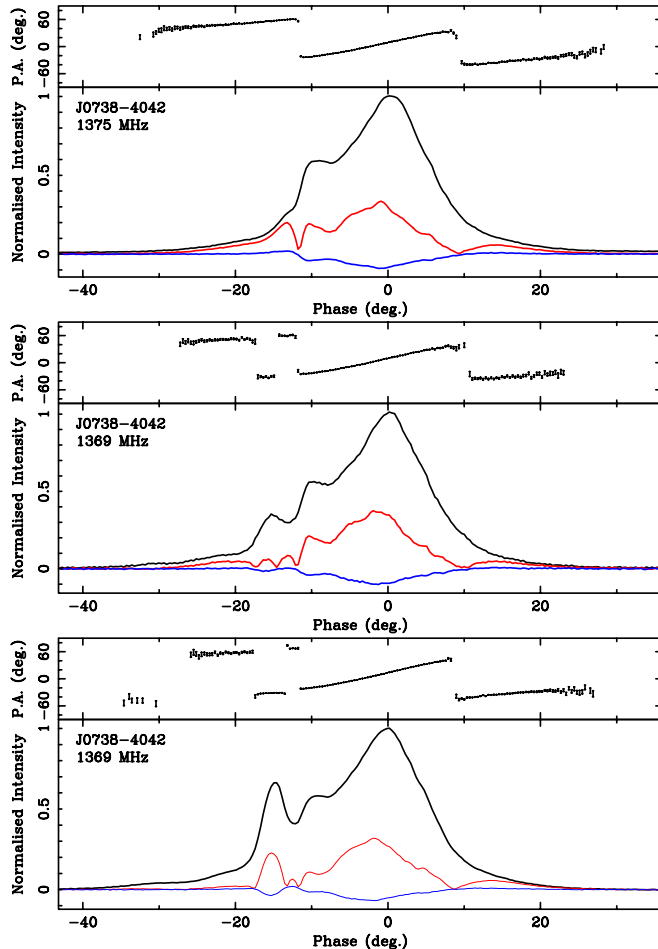


**Figure 3.** Three average profiles of PSR J0738–4042 in full polarization, from 2004, 2006 and 2010 (top to bottom). The total intensity (black), linear polarization (red) and circular polarization (blue) are shown just below the PA curve (dotted line). The extra component in the 2006 and 2010 profiles is clearly responsible for the observed additional orthogonal jumps in the leading edge of that profile. These jumps coincide in phase with local minima in the linear polarization.

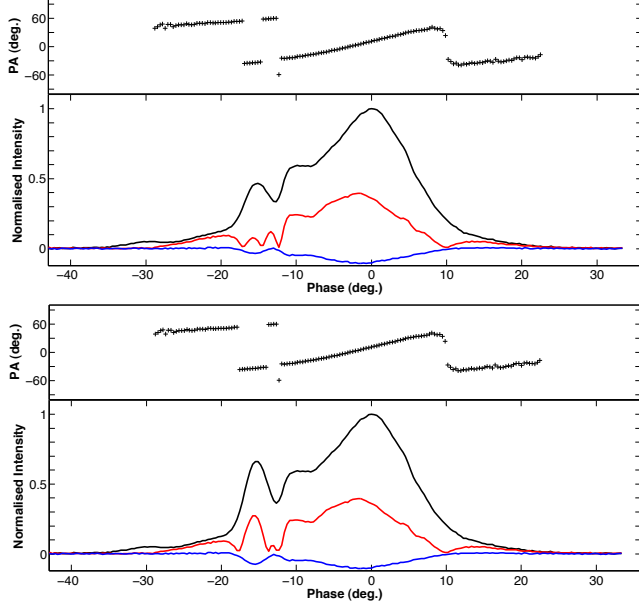


**Figure 4.** Simulated polarization profiles resembling the data of 2006 and 2010 from Fig. 3. These profiles have been generated by adding an orthogonally polarized, Gaussian component of fixed width and variable amplitude to the polarization profile without the transient component (from 2004). Most features of Fig. 3 around pulse phase  $-15^\circ$  are well reproduced.

Between pulse phase  $-20^\circ$  and  $-10^\circ$ , there are 3 orthogonal polarization jumps in the 2006 and 2010 profiles, as opposed to a single jump in the 2004 data. It is also evident that the degree of linear polarization in this region of the profile is related to the total power, and that there are local minima directly related to the orthogonal PA jumps. A comparison between the 2004 and 2006 data shows that as the total power increases around pulse phase  $-16^\circ$ , the linear polarization drops.

We attempted to reproduce the observed changes in polarization using a simple model. The starting point of the model is the polarization profile obtained from observations in 2004 shown at the top of Fig. 3. To this, we added a Gaussian component centred at phase  $-15.47^\circ$ , which is 100% polarized. We computed the total intensity  $I_c$  of the simulated component as:

$$I_c(\phi) = A \exp[-(\phi - 15.47)^2 / (2\sigma^2)], \quad (1)$$

where  $A$  the amplitude and  $\sigma$  the width of the Gaussian, and  $\phi$  the pulse phase. For each pulse phase bin, we set the polarization of the simulated component to be orthogonal to the polarization of the 2004 profile, by computing its Stokes parameters ( $I_c, Q_c, U_c, V_c$ ) relative to the Stokes parameters of the 2004 profile ( $I_o, Q_o, U_o, V_o$ ), taking into account that:

$$\frac{U_c}{Q_c} = \frac{U_o}{Q_o}, I_c = \sqrt{Q_c^2 + U_c^2 + V_c^2} \quad (2)$$

Therefore,  $Q_c$ ,  $U_c$  and  $V_c$  can be computed for every pulse phase bin as:

$$Q_c = -\frac{Q_o I_c}{\sqrt{Q_o^2 + U_o^2 + V_o^2}} \quad (3)$$

$$U_c = -\frac{U_o I_c}{\sqrt{Q_o^2 + U_o^2 + V_o^2}} \quad (4)$$

$$V_c = -\frac{V_o I_c}{\sqrt{Q_o^2 + U_o^2 + V_o^2}} \quad (5)$$

where the  $-$  signs ensure that the polarization vectors are antiparallel on the Poincaré sphere. Finally, we add the Stokes parameters of the new component to the 2004 data to produce simulated polarization profiles.

Figure 4 shows the best results of our model, which can be compared directly to Fig. 3. We find that we can reproduce the data very closely by setting  $\sigma = 1.43^\circ$  and varying  $A$  between  $\sim 0.25$  for the 2006 data and  $\sim 0.5$  for the 2010 data. The fact that, at the relevant pulse phase region, the 2004 profile is almost entirely polarized, and the 2006 and 2010 profiles can be simulated by adding a 100% and orthogonally polarized component leads to the conclusion that the polarization profiles with the additional component are direct observations of the superposition of two, 100% polarized, orthogonal modes of emission.

## 4 STATISTICAL DESCRIPTION OF THE PROFILE EVOLUTION

### 4.1 Hidden Markov models

Visual inspection of the profiles of Fig. 2 suggests that the profile evolution of PSR J0738–4042 can be described by a single change of state, an assertion that is supported by the polarization modelling described in the previous section. We utilize a fully probabilistic realization of a hidden Markov model (HMM) to automatically identify putative state changes in the data. Hidden Markov models (Rabiner 1989) have been widely used for inferring latent changes in sequential data. Consider a sequence of observations,  $\mathbf{Y} = \{\mathbf{y}_t\}_{t=1}^T$ ,  $\mathbf{y}_t \in \mathbb{R}^d, \forall t$ . The distribution of an observation,  $\mathbf{y}_t$  is determined by a corresponding *hidden* state,  $s_t \in \{1, \dots, J\}$  and a state dependent observation probability.

The hidden state at time  $t = 1$  is determined by a prior state vector,  $\boldsymbol{\pi} = [\pi_1, \dots, \pi_J]^T$ , where  $\pi_j = p(s_1 = j)$ . The *Markov property* implies that a hidden state  $s_{t-1}, s_t$  depends only on  $s_{t-1}$  and not on those at time  $t - 2$  and before:

$$p(s_t | s_{t-1}, \dots, s_1) = p(s_t | s_{t-1}). \quad (6)$$

State transitions are jointly determined by a transition matrix,  $\mathbf{A} = [a_{ij}]$ , where  $a_{ij} = p(s_t = j | s_{t-1} = i)$  and observation likelihoods. An observation  $y_t$  depends only on the corresponding hidden state,  $s_t$  and we utilize here a state-dependent Gaussian density, such that the predictive distribution over observations, conditioned on the hidden state, is given by:

$$p(\mathbf{y}_t | s_t = j) = \mathcal{N}(\mathbf{y}_t; \boldsymbol{\mu}_j, \boldsymbol{\Sigma}_j), \quad (7)$$

where  $\boldsymbol{\mu}_j$  and  $\boldsymbol{\Sigma}_j$  are the mean vector and a covariance matrix for the  $j^{\text{th}}$  state.

Inference in a HMM proceeds by evaluation of the posterior distribution over the parameters,  $\{\boldsymbol{\pi}, \mathbf{A}, \boldsymbol{\mu}, \boldsymbol{\Sigma}\}$  as well as the posterior distributions of the hidden state variables,  $p(s_t | \mathbf{Y})$ . A two-stage maximum-likelihood algorithm is often adopted, such as the Baum-Welch algorithm (Baum et al. 1970), a special case of the expectation-maximisation (EM) algorithm (Dempster et al. 1977). The most probable state-sequence can be found using the Viterbi algorithm (Rabiner

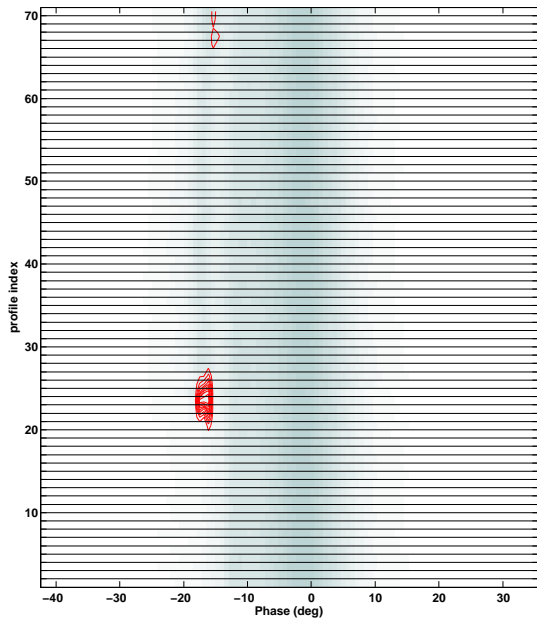


**Figure 5.** Contours of the entropy of the HMM, superposed on the profiles from Fig. 2. The entropy is a measure of the probability of a state change, and reaches the value 1 in profile 23 and pulse phase -16. The contours are at entropy value steps of 0.1, from 0 to 1. Apart from profile 23, the probability of a state change is increased in profile 68.

1989). The maximum-likelihood approach, however, has major limitations; most notably overfitting and inference of underlying model complexity, such as determining the most probable number of states. In order to address these limitations, we employ a fully Bayesian approach, which exploits the tractable bounds of *variational Bayes* approximations (Jordan et al. 1999). The Bayesian methodology allows for uncertainty to be handled at all levels of inference, making the approach ideal for analysis of smaller data samples. Furthermore, the number of underlying states is inferred automatically such that sequences without significant state changes are modeled by a single state process. This deviates significantly from maximum-likelihood methods in which the data is forced into a set number of states.

As posterior state probabilities are inferred for each datum, we can investigate with ease not only the existence of state changes but also track the entropy associated with state determination at each point. The information entropy associated with the posterior over the states, conditioned on observation  $\mathbf{y}_t$  is hence given as:

$$\mathcal{H}_t = - \sum_j p(s_t = j | \mathbf{y}_t) \log p(s_t = j | \mathbf{y}_t). \quad (8)$$

The advantage of utilizing entropy lies in the fact that increases in entropy will occur in locations in which a full state-change is not supported by the data. If the logarithm is to base two, then the entropy is returned in *bits*, with 1 bit of entropy indicating the existence of a fully supported state change.

We use the Bayesian HMM to infer the posterior dis-

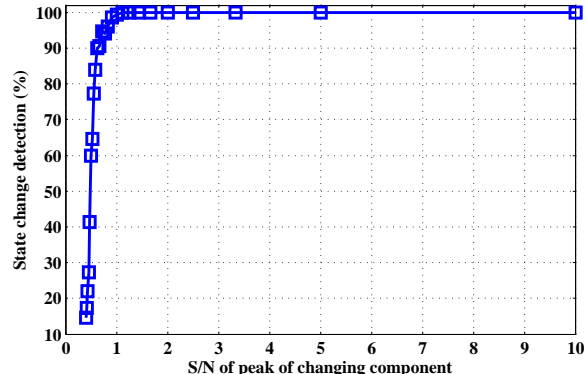


**Figure 6.** Results of the sensitivity analysis. The curve shows the fraction of 1000 simulated profiles where the HMM successfully identifies a state change, versus the S/N of the new component. The HMM performs perfectly for S/N of 1 and above.

tribution over the state sequence for each bin of the pulse profile, using the total power amplitudes of each bin as our observables. Figure 5 shows the entropy (in bits) of the state posterior applied to all bins of all profiles, in contours superposed on the raw data. The contours, which range from 0 to 1 in steps of 0.2, indicate very high probability of a state change in profile 23, but also suggest there may be further change in the most recent observations (profile 68). Artificially changing the order of the profiles moves the identification point of the state change accordingly.

## 4.2 Sensitivity analysis

Although the HMM clearly and robustly identifies a state change in the average pulse profile, it is not surprising that this analysis performs well, given the large magnitude of the event (it can be picked out clearly by eye). We have performed a sensitivity analysis to test the performance of the HMM on noisier data. This involves adding increasing levels of white noise to the profiles and comparing the state-change identification with the original analysis. We have performed this analysis by means of a Monte Carlo simulation, producing 1000 versions of each profile with a given S/N and changing the noise from 4 to 100 times the original in steps of 4 (i.e.  $25 \times 10^3$  simulated profiles for each observed profile). For each set of profiles at a given S/N, we run the HMM and count the fraction of sets in which a state change is detected, as well as the profile number that the transition occurs.

Figure 6 shows the results of the sensitivity analysis, as the fraction of the 1000 sets where a state change is detected, versus the S/N of the peak of the new component in the simulated data. Addition of the noise levels mentioned above artificially decreases the average S/N of the peak of the new component to values between 0.4 and 10. The HMM performs extremely well from S/N per pulse phase bin of 1 and above.

## 5 DISCUSSION AND CONCLUSIONS

We have shown that PSR J0738–4042 has undergone dramatic changes in its average pulse profile in the period between 2004 and 2006. The changes affect the total amplitude and polarization of a single component on the leading edge of the profile and are broadband at least over the frequency range between 600 and 3100 MHz. Examination of the literature shows that the transient component was present between 1970 and 1990, then absent until 2006 since when it has again been present up to the current epoch (January 2011). The ‘intermittency’ of this particular component can therefore be measured in tens of years compared to e.g. the tens of days in PSR B1931+24. This serves as a unique example of magnetospheric changes on very long time scales. This is further proof that there remains a lot to be understood on the dynamic nature of pulsar magnetospheres on all timescales.

The increase in intensity of the transient component is accompanied by an orthogonal transition in the position angle of the linear polarization, and by a decrease in the fractional linear polarization of that part of the profile. When the extra component is absent the leading part of the profile is almost completely polarized. Orthogonal jumps in the polarization angle are common in pulsars with medium or low levels of linear polarization, which implies that the degree of polarization is affected by the presence of the two modes. In the past, two models have been put forward to account for this behaviour: the observed pulsar radiation either occurs in two partially polarized orthogonal modes of emission which are emitted disjointly (e.g. Cordes et al. 1978), or two entirely polarized orthogonal modes, the superposition of which sets the total polarization (eg McKinnon & Stinebring 2000). The data presented here strongly favour the latter, as this is the first example where we see two distinct states: a single mode and high polarization when the additional component is absent, and low polarization associated with higher total intensity when it appears. We show the validity of this interpretation of the post-2006 data with a simple simulation.

Orthogonal polarization modes are thought to be related to propagation effects within the pulsar magnetosphere (e.g. Melrose 2000), which then strongly suggests a magnetospheric rather than geometric origin for the observed profile changes. We consider a geometrical effect such as free precession to be extremely unlikely. Magnetospheric effects have been shown to be responsible for the profile changes seen in PSR B1931+24, and the correlations between the period derivative and the profile shape changes of a small number of pulsars in Lyne et al. (2010) also point to magnetospheric effects. In PSR J1119–6127, profile changes seem to occur immediately following a glitch (Weltevredre et al. 2010). Although there are insufficient existing data to trace the behaviour of the timing of the pulsar over the long term, there is no evidence for glitch activity between 2004 and 2006. Also, unlike PSR J1119–6127, a long series of single pulses from PSR J0738–4042 taken after 2006 shows the transient component to be persistent in the single pulses with no more than typical variability.

We have presented a robust statistical technique based on a Hidden Markov Model that estimates the likelihood of state changes in the total power data, and showed that this

technique has great potential for substantially noisier data in which similar systematic changes occur. We plan to apply the HMM technique to a large number of pulsars for which regular observations have been conducted, to look for and characterise statistically significant profile variations. Most importantly, this technique provides a means of correlating changes in the pulse profile with other physical parameters, such as the period and period derivative, which could prove extremely useful in partially accounting for non-Gaussian timing residuals in pulsar timing models.

## ACKNOWLEDGMENTS

AK is grateful to the Leverhulme Trust for financial support. The Australia Telescope is funded by the Commonwealth of Australia for operation as a National Facility managed by the CSIRO.

## REFERENCES

- Backer D. C., 1976, *ApJ*, 209, 895  
 Baum L. E., Petrie T., Soules G., Weiss N., 1970, *Ann. Math. Stat.*, 41, 164171  
 Cordes J. M., Rankin J. M., Backer D. C., 1978, *ApJ*, 223, 961  
 Dempster A. P., Laird N. M., Rubin D. B., 1977, *J. Roy. Stat. Soc. B Met.*, 39, 1  
 Gil J. A., Jessner A., Kijak J., Kramer M., Malofeev V., Malov I., Seiradakis J. H., Sieber W., Wielebinski R., 1994, *A&A*, 282, 45  
 Hobbs G., 2008, *Classical and Quantum Gravity*, 25, 114032  
 Johnston S., Karastergiou A., Willett K., 2006, *MNRAS*, 369, 1916  
 Johnston S., Kramer M., Karastergiou A., Hobbs G., Ord S., Wallman J., 2007, *MNRAS*, 381, 1625  
 Jordan M. I., Ghahramani Z., Jaakkola T. S., Saul L. K., 1999, *Mach. Learn.*, 37, 183  
 Karastergiou A., Johnston S., 2006, *MNRAS*, 365, 353  
 Karastergiou A., Johnston S., Manchester R. N., 2005, *MNRAS*, 359, 481  
 Karastergiou A., Kramer M., Johnston S., Lyne A. G., Bhat N. D. R., Gupta Y., 2002, *A&A*, 391, 247  
 Komesaroff M. M., Morris D., Cooke D. J., 1970, *Astrophys. Lett.*, 5, 37  
 Kramer M., 1998, *ApJ*, 509, 856  
 Kramer M., 2008, in C. Bassa, Z. Wang, A. Cumming, & V. M. Kaspi ed., *40 Years of Pulsars: Millisecond Pulsars, Magnetars and More* Vol. 983 of American Institute of Physics Conference Series, *Observations of Pulsed Emission from Pulsars*. pp 11–19  
 Kramer M., Lyne A. G., O’Brien J. T., Jordan C. A., Lorimer D. R., 2006, *Science*, 312, 549  
 Large M. I., Vaughan A. E., Wielebinski R., 1968, *Nature*, 220, 753  
 Lorimer D. R., Kramer M., 2005, *Handbook of Pulsar Astronomy*. Cambridge University Press  
 Lyne A., Hobbs G., Kramer M., Stairs I., Stappers B., 2010, *Science*, 329, 408

- McCulloch P. M., Hamilton P. A., Manchester R. N., Ables J. G., 1978, MNRAS, 183, 645
- Manchester R. N., Hamilton P. A., McCulloch P. M., 1980, MNRAS, 192, 153
- Manchester R. N., Kramer M., Stairs I. H., Burgay M., Camilo F., Hobbs G. B., Lorimer D. R., Lyne A. G., McLaughlin M. A., McPhee C. A., Possenti A., Reynolds J. E., van Straten W., 2010, ApJ, 710, 1694
- McKinnon M. M., Stinebring D. R., 2000, ApJ, 529, 435
- McLaughlin M. A., Lyne A. G., Lorimer D. R., Kramer M., Faulkner A. J., Manchester R. N., Cordes J. M., Camilo F., Possenti A., Stairs I. H., Hobbs G., D’Amico N., Burgay M., O’Brien J. T., 2006, Nature, 439, 817
- Melrose D. B., 2000, in Kramer M., Wex N., Wielebinski R., eds, Pulsar Astronomy - 2000 and Beyond, IAU Colloquium 177 The status of pulsar emission theory. Astronomical Society of the Pacific, San Francisco, p. 721
- Noutsos A., Karastergiou A., Kramer M., Johnston S., Stappers B. W., 2009, MNRAS, 396, 1559
- Rabiner L. R., 1989, Proc. IEEE, 77, 257
- Sedrakian A., Wasserman I., Cordes J. M., 1999, ApJ, 524, 341
- Smits J. M., Stappers B. W., Edwards R. T., Kuijpers J., Ramachandran R., 2006, A&A, 448, 1139
- Stairs I. H., Lyne A. G., Shemar S., 2000, Nature, 406, 484
- van Ommen T. D., D’Alessandro F. D., Hamilton P. A., McCulloch P. M., 1997, MNRAS, 287, 307
- Weisberg J. M., Taylor J. H., 2002, ApJ, 576, 942
- Weltevrede P., Johnston S., 2008, MNRAS, 391, 1210
- Weltevrede P., Johnston S., Espinoza C. M., 2010, ArXiv e-prints